Scientific report; 97 - 08

KNMI

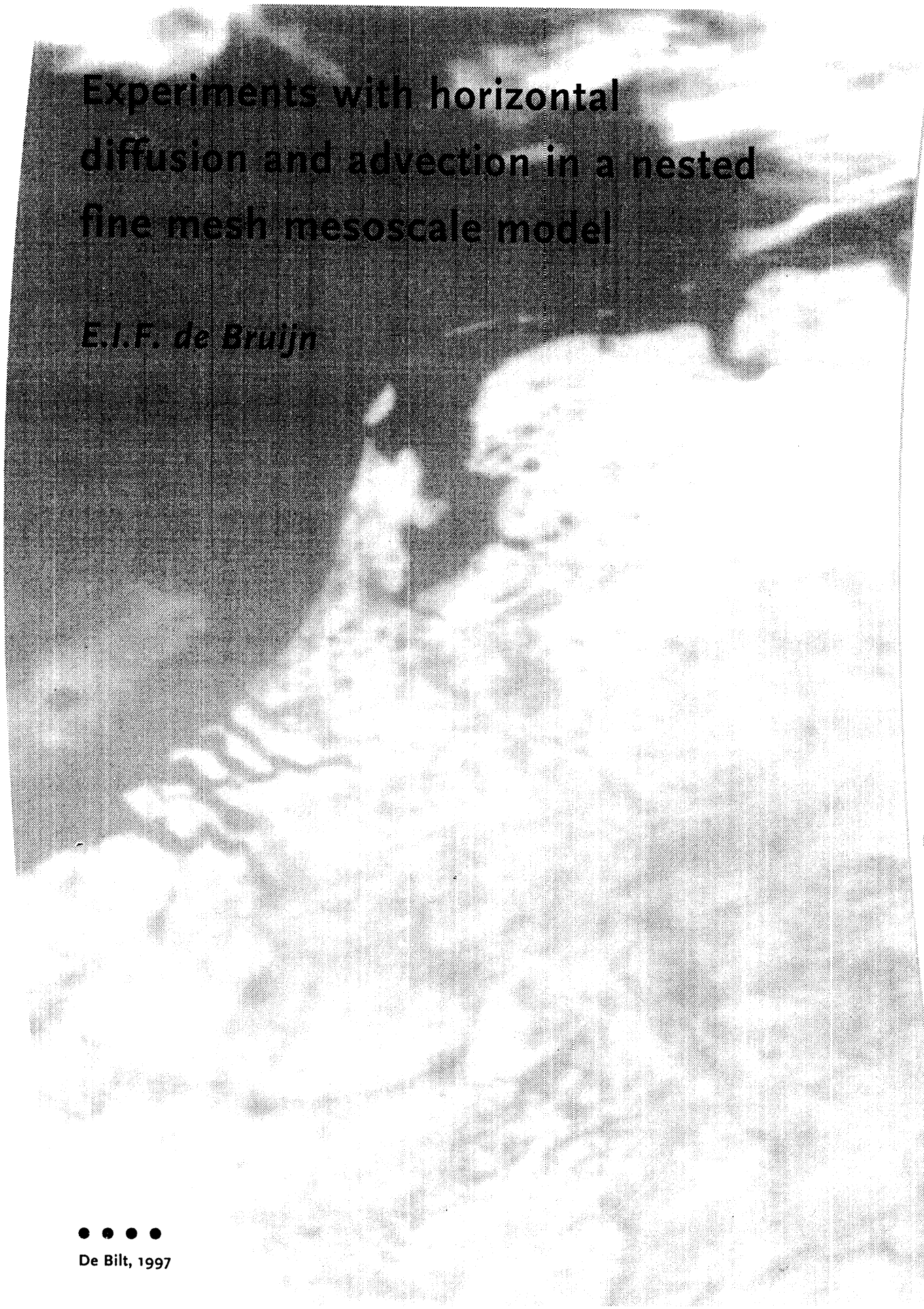

Experiments with horizontal diffusion and advection in a nested fine mesh mesoscale model

E.I.F. de Bruijn

De Bilt, 1997

Koninklijk Nederlands Meteorologisch Instituut

Scientific report = wetenschappelijk rapport; WR 97 - 08

De Bilt, 1997

PO Box 201
3730 AE De Bilt
Wilhelminalaan 10
De Bilt
The Netherlands
Telephone + 31(0)30-220 69 11
Telefax + 31 (0)30-221 04 07

Author: E .I.F. de Bruijn

UDC: 551.511.3
551.516
551.509.3

ISSN: 0169-1651

ISBN: 90-369-2129-5

● ● ● ●

Experiments with horizontal diffusion and advection in a nested fine mesh mesoscale model

E.I.F. de Bruijn
KNMI
November 1997

email: bruijnde@knmi.nl
tel: + 31 30 2206813

Contents

1 Samenvatting **2**

2 Introduction **3**

3 Background **5**

3.1 Basics and relevant model details 5

3.2 Horizontal diffusion 7

3.3 Atmospheric spectra 9

4 A case study **11**

4.1 General aspects of the sea breeze circulation 11

4.2 Sensitivity for diffusion 11

4.3 Eulerian versus semi-Lagrangian advection scheme 14

4.4 Impact of the stepsize of nesting 18

4.5 Meteorological details with the most suitable model 25

5 Conclusions and recommendations **29**

6 Acknowledgements **30**

A a and b coefficients hybrid coordinate system **32**

1 Samenvatting

Recent is een hoge resolutie versie van het HIRLAM met een roosterpuntsafstand van 5.5 km op het KNMI beschikbaar gekomen. De instelling van belangrijke modelgrootheden zoals horizontale diffusie, roosterpuntsafstand, tijdstap en de keuze van advectieschema dienen zorgvuldig bepaald te worden.

In dit rapport wordt een methode om de modeluitvoer te interpreteren ontwikkeld. Velden van de windsnelheidscomponenten worden spectraal geanalyseerd. Als hun spectrum niet afvalt volgens een $-5/3$ macht, is dat een aanwijzing dat er fysisch onrealistische processen plaatsvinden in het model. Een case-studie van 29 juli 1995 is gekozen omdat er op die dag weinig wind was en het zeewindeffect werd waargenomen. Modelruns met theoretisch afgeleide waardes voor de horizontale diffusie coefficienten geven geen goede resultaten. Op basis van subjectieve veldverificatie en het spectrale gedrag blijkt dat meer horizontale diffusie nodig is.

Zowel het Euleriaanse als het semi-Lagrangriaanse advectieschema zijn bruikbaar voor de simulatie van de zeewindcirculatie. Echter het semi-Lagrangriaanse schema is gevoeliger voor numerieke ruis, maar heeft minder rekentijd nodig. Kunstmatige golven afkomstig van het opleggen van de randvoorwaarden blijken in het model voor te komen. Door bij de randen te filteren, zodat alleen de grootschalige informatie overblijft, wordt de numerieke ruis verwijderd. De resolutie in het geneste model kan tien keer verhoogd worden.

Uiteindelijk geeft het semi-Lagrangriaanse advectieschema met gefilterde randen bevredigende resultaten. Met dat systeem worden de meteorologische verschijnselen in Valkenburg (vliegveld bij Den Haag) en in Cabauw bestudeerd. Het zeewindeffect met de typische winddraaiing en de temperatuursprong worden door het model gerepresenteerd, hoewel het model een fasefout vertoont.

2 Introduction

Successful mesoscale forecasts are desirable for the improvement of regional weather forecasts. Considerable efforts have been put into the development of an operational mesoscale forecasting system. For instance, Nielsen (1995) [8] described examples of forecasts obtained from a nested mesoscale model at the Danish Meteorological Institute. The potential and problems associated with high-resolution forecasts are discussed. Clarke (1991) [1] reported about some nesting procedures. One-way nesting means that large scale information is fed in the embedded nested model, but the computional results are not returned to the larger scale model. The two-way nesting method allows the feed-back of modified high resolution data to the larger scale model.

At KNMI a high resolution model has been developed, but the nesting strategy and the performance of the advection scheme has never been evaluated. The lateral boundaries of the high resolution model are predescribed by the coarser grid model. It is not clear whether a very high resolution model with a grid size of 5 kilometers can be embedded directly in the 55 kilometer HIRLAM. Perhaps an intermediate model is necessary.

Another question is whether the large scale energy is correctly fed into the high resolution model. The dynamical part of the model can be described by a Eulerian or semi-Lagrangian advection scheme. The performance and efficiency of the advection schemes have never been studied in high resolution models at KNMI. In addition the setting of model parameters such as the timestep and the horizontal diffusion coefficients have never been checked. The values of the horizontal diffusion coefficients can be derived theoretically, but experimentation is still required to obtain optimal results.

The semi-Lagrangian scheme offers advantages with respect to computer-time, but the performance in high resolution models is unknown. Generated noise can be removed from the fields by horizontal diffusion. However to much smoothing leads to the loss of useful information. The semi-Lagrangian scheme is described by McDonald and Haugen (1992) [5] and McDonald and Haugen (1993) [6] and is currently applied in HIRLAM.

A method for testing and judging the model results will be developed. At first subjective verification is used to examine the model output. In addition Fourier analysis is applied to construct energy spectra. Spectra are decompositions of the model fields into waves of different wavelengths and thus give an idea about the way how waves of different sizes exchange energy

with each other. Energy is produced on the synoptic scale, then transported to smaller scales in the so-called inertial subrange, and finally dissipated on molecular scales. The spectrum in the inertial subrange should decay in intensity according to a $-5/3$ power law Tennekes (1972) [9].

Due to the limited grid size the process of dissipation is parameterized. Horizontal diffusion is prescribed. The adding of horizontal has the effect of damping the 2-4 grid point waves. Therefore horizontal diffusion will weaken sharp gradients in the model forecasted fields. It is apparent that allowing for too much diffusion will lead to a loss of details of the small scales. The choice of the horizontal diffusion coefficient will be tested by examining the decay of the spectrum and by subjective verification of the model fields in the boundary layer and in the free atmosphere. Near the surface more small scale phenomena are expected than aloft.

Below we start with the description of the nested models. Then some background is given about the specification of the horizontal diffusion coefficient and time step with respect to the varying grid size. Further the method of calculating spectra with its inherent difficulties is explained. In section 4 a case-study with quiet weather phenomena i.e. no passing of frontal depressions, is selected for testing and optimizing the setting of the model parameters. The area of interest is the Netherlands which does not have mountains and the land-sea distribution is rather inhomogenous. Subsequently the sensitivity-analysis for horizontal diffusion is described, followed by experiments with varying grid sizes. The results with the semi-Lagrangian and Eulerian advection schemes in relation with horizontal diffusion coefficients are reported. Finally attention is paid to the filtering of the boundary fields and the stepsize of the increase of the horizontal resolution. The model with the best performance is used to study the meteorological situation in more detail and we conclude in section 5.

3 Background

3.1 Basics and relevant model details

In an atmospheric model the governing equation for a variable X can be schematically written as

$$\frac{\partial X}{\partial t} = D_x + P_x + K_x \tag{1}$$

where X may represent the horizontal windcomponents (u,v), the temperature (T) or the specific humidity (q). D_x represent the dynamical tendencies, P_x tendencies from the physical parametrization of variable X and K_x expresses the tendency due to the horizontal diffusion.

In this study we focus on the dynamics and the horizontal diffusion. To solve the dynamics two advection schemes are available, the Eulerian and the semi-Lagrangian scheme. The implementation of the scheme on a limited area is described by McDonald and Haugen (1992) [5]. The model is based on primitive equations and a sophisticated physics package is incorporated. In McDonald and Haugen (1993) [6] the model is extended to hybrid vertical coordinates. The semi-Lagrangian approach offers advantages in accuracy and stability that cannot be obtained from the Eulerian scheme. The semi-Lagrangian method enables the integration of horizontal and vertical advection terms with an unconditionally large time step. Therefore the scheme is computationally more efficient than the Eulerian scheme and thus attractive to be applied in very high resolution models.

At KNMI HIRLAM provides daily forecasts for operational practice. HIRLAM has a gridpoint distance of 55 kilometer and is from now on appointed as V55. Within V55 two nested models are defined, namely V20 and VHR with gridsizes of 20 and 5 kilometer, respectively.

In Fig. 1 the integration areas of the three models are presented. All models have a rotated latitude-longitude grid with the South Pole at (30 S, 180 E). The models are encoded on an Arakawa-C grid, meaning that u,v and T are staggered in the horizontal. In the vertical plane a hybrid coordinate system is defined as follows

$$P_i = A_i + B_i \cdot P_s \tag{2}$$

P_i is the pressure at model level i, A_i,B_i are the coefficients which determine the closeness of the system to σ-coordinates (A_i=0) or p-coordinates (B_i=0)

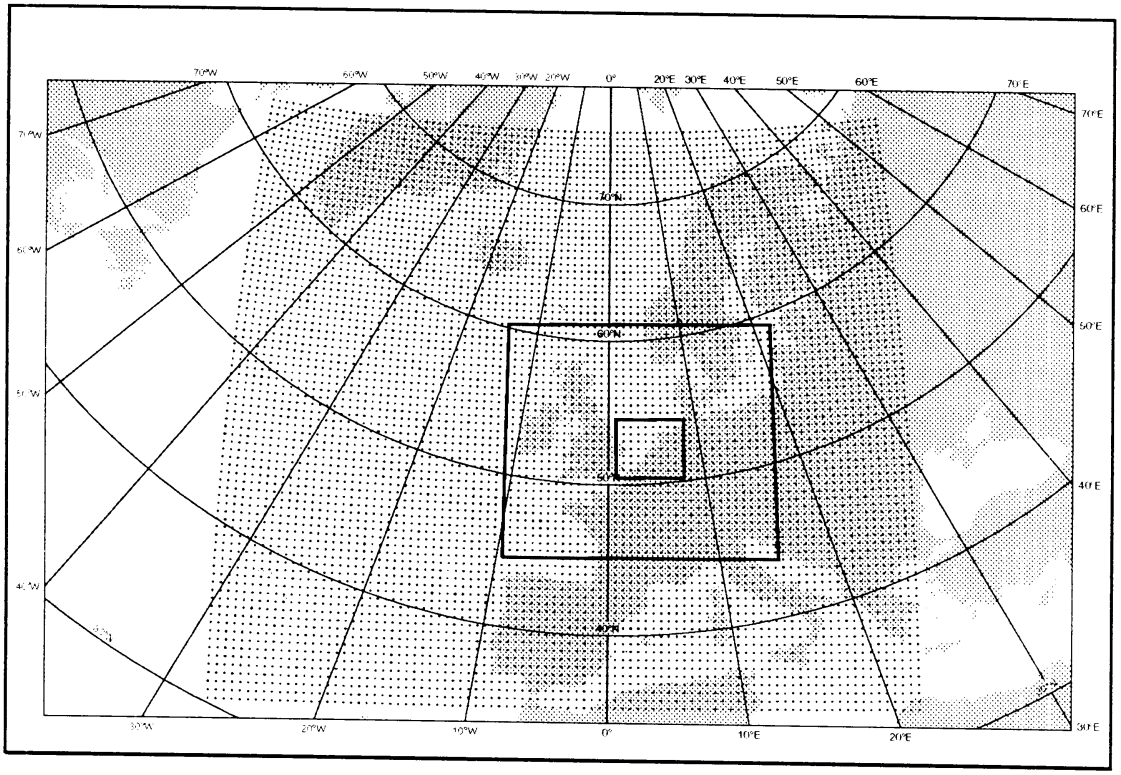

Figure 1: The integration areas for V55 (large), V20(medium) and VHR (small)

and P_s is the surface pressure. See appendix A for values of A_i and B_i used in the models. The vertical coordinate system is non-orthogonal and terrain following and the vertical spacing is defined with 6 levels below a height of 2000 m. It is obvious that the basic differences concern the horizontal resolution and the size and position of the integration area.

The analysis is performed on the largest scale namely in the V55 model. The nested models do not have their own analysis scheme and receive their initial information from the coarse mesh model. Prior to the forecast an implicit normal mode initialization with four vertical modes using adiabatic model tendencies and two iterations is made Haugen (1991) [4]. The lateral boundary fields are changed every time step using a relaxation scheme over eight interior boundary lines. The frequency of the new boundary fields is three hours. At intermediate times the boundary values are interpolated

linearly.

The directly nested models use interpolated analyzed fields as boundary conditions. V20, which does not have its own analysis scheme produces forecasted fields which are used as boundary fields for the doubly nested VHR. Every hour boundary information, based on predicted fields are fed to the inner model.

The physical parameterizations schemes are described by Gustafsson (1991) [3]. Some relevant parts of the physics work as follows. Surface fluxes are determined by means of a drag coefficient formulation, using Monin-Obukov similarity theory for the atmospheric surface layer. The calculation of fluxes above lowest model level is based on mixing length formulation using exchange coefficients that depend on the static stability, which is described by means of a Richardson number. Surface processes are included by simple prognostic equations. Soil water and temperature are described in three layers, with climatogical values assigned to the deepest layer. The climatological information are derived from the V55 model. The roughness length however, is updated for VHR using wind climate data of Wieringa (1995) [10].

In this research we concentrate on the dynamics and the horizontal diffusion in the nested models. The horizontal diffusion is necessary to control the noise in the fields and to obtain stable integrations. In the following paragraph some background is given on this issue.

3.2 Horizontal diffusion

The dynamical part D_x from equation (1) can be solved with a Eulerian and a semi-Lagrangrian advection scheme. In both cases the equations contain a term for horizontal diffusion, because the noise has to be filtered in order to keep the fields smooth. In order to diffuse the field 'X' we wish to solve the equation

$$\frac{\partial X}{\partial t} - K\nabla^2\nabla^2 X = 0 \tag{3}$$

where K is the diffusivity coefficient and ∇^2 the Laplacian.

Due to the large time step used in the semi-Lagrangian integrations an implicit scheme has to be used for the numerical solution in order to maintain numerical stability. Because of the complexity of the implicit fourth order diffusion scheme, the numerical stability, e-folding and diffusion coefficient are explained on the basis of the explicit fourth order diffusion scheme. In

case of an explicit leapfrog time differencing scheme the diffusion equation becomes

$$X^{n+1} = X^{n-1} + 2\Delta t K \nabla^2 \nabla^2 X^{n-1} \tag{4}$$

The response function R is defined as $\bar{X}/X$ where $\bar{X}$ refers to the diffused values. When a two dimensional wave solution in discrete fashion

$$X(x, y, t) = A(t) exp(i(nk\Delta x + ml\Delta y)) \tag{5}$$

is substituted in (4), an expression for R can be derived. k and l are wavenumbers in the x and y direction, respectively. After some algebra the following expression for the response function R can be found

$$R = 1 - \frac{32\Delta t K}{a^4}[\frac{1}{\Delta x^2} sin^2(\frac{k\Delta x}{2}) + \frac{1}{\Delta y^2} sin^2(\frac{k\Delta y}{2})]^2 \tag{6}$$

Details about this exercise and more specifically about the finite difference approximation can be found in Eerola (1993) [2]. Numerical stability and no phase shift conditions require that $0 \leq |R| \leq 1$. From eq.(6) the e-folding time and the diffusion coefficient can be derived. The e-folding time is the time interval where the amplitude of a wave number k,l is damped to 1/e times the initial value.

$$T_e = -\frac{\Delta t}{ln(R)} \tag{7}$$

On small scales with wave lengths of two grid boxes the e-folding is small. This means that those waves damp relatively quick. Conversely larger waves are less affected resulting in longer e-folding times. The diffusion coefficient is strongly related with the e-folding time and can also be determined from the response function

$$K = \frac{a^4 \Delta x^4}{128 \Delta t sin^4(\frac{k\Delta x}{2})}(1 - e^{-2\frac{\Delta t}{T_e}}) \tag{8}$$

where a is the radius of the earth multiplied with a metric coefficient.

From the above equations it is obvious that if the timestep or the grid length is changed, the diffusion coefficient K must also be changed to keep the amount of diffusion the same. For practical experimentation a useful relation can be obtained from (8). When we assume a two-gridpoint wave

($k = \frac{\pi}{\Delta x}$) and an e-folding time $T_e = n \cdot \Delta t$ with $n = 1$ or $n = 2$ the relation between K_1 and K_2 for two-gridpoint waves becomes

$$\frac{K_1}{K_2} = \frac{\Delta t_2}{\Delta t_1}(\frac{\Delta x_1}{\Delta x_2})^\gamma \tag{9}$$

where γ is the order of the diffusion scheme. In practice larger wave lengths should be damped as well and for the e-folding time 10 minutes is chosen. Therefore the scaled down K coefficient will be underestimated and a slight increase is required (see also 4.4). It should be noted that the simplified scaling down formula (9) can be applied for higher order diffusion schemes when γ is modified.

3.3 Atmospheric spectra

The spectral decay of the flow is a signature of the energy housekeeping and deviations may indicate irregularities in the numerical model, for instance the development of artificial waves and reflections at the lateral boundaries. The data in the domain can be seen as a sum of individual waves with differing wavelengths. First we define $s(\vec{x})$ as the amplitude of the meteorological data, for instance the u-component of the wind. It should be noted that s is a function of $\vec{x}$. However for the spectral analysis we want to obtain s as a function of the wave vector $\vec{k}$. Therefore the transformation is carried out by evaluating the Fourier integral

$$s(\vec{k}) = \int_{-\infty}^{\infty} s(\vec{x}) e^{i\vec{k}\vec{x}} dx \tag{10}$$

and neglecting trivial factors of 2π. However this integral has to be estimated on a limited discrete horizontal domain. The wave lengths vary between 10 and 320 kilometers. The integral is computed numerically by summing the individual wave components along the x- and y-axis using a Fast Fourier Transform (FFT). The FFT expects a periodic and a two dimensional field in which the number of grid points in one direction should be a power of two. The field is prepared for the FFT by selecting a square of 64 by 64 points from the middle of the original field and periodicity is assumed. As a result the data in the boundary zone is not accounted for in the spectral analysis.

The FFT gives spectral components which are dependent on direction. The power spectrum is computed by performing the polar integration

$$E(k) = \int_0^{2\pi} \mid \hat{s}(\vec{k}) \mid^2 k \; d\phi \tag{11}$$

where $k = \mid \vec{k} \mid$, and this integral is solved numerically. First the integral is transformed to cartesian coordinates in terms of orthogonal components of the wave vector $\vec{k}$.

$$E(k) = \int_{k_1=0}^{\infty} \int_{k_2=0}^{\infty} \mid \hat{s}(\vec{k}) \mid^2 \delta(\sqrt{k_1^2 + k_2^2} - k) dk_1 dk_2 \tag{12}$$

The term $\delta(\sqrt{k_1^2 + k_2^2} - k)$ accounts for the integration of the Fourier components along the radius k. Due to the discrete FFT $\vec{k}$ is not continuous. Therefore the integral has to be discretely summed as follows

$$E(k) = \sum_{i=0}^{k_{nx}} \sum_{j=0}^{k_{ny}} \mid \hat{s}(k_{ix}, k_{jy}) \mid^2 \delta(\sqrt{k_{ix}^2 + k_{jy}^2} - k) \tag{13}$$

where $k = int(\sqrt{k_{ix}^2 + k_{jy}^2})$ and k_{ny},k_{nx} are the maximal indices corresponding to the Nyquist frequencies for the two components of the wavevector. It should be noted that E(k) gains more accuracy for higher frequencies i.e. smaller wavelengths. In the complex space in which the summation is carried out, the density of discrete k values increases when the Nyquist frequency is approached and thus the summation can be better estimated.

After setting up a system for computing spectra, the method was checked roughly by a comparison between model output and observations. The zonal and meridional windcomponents at a pressure level of 200 hPa were compared with aircraft observations Nastrom et al (1984) [7]. They used data of period of 8 years for a global area with an average latitude of 50 degrees. They discovered that the spectrum obeys a -5/3 power law dependence on wavenumber over the wavelength range 2.6-300 km and a -3 power law over the wavelength range 1000-3000 km. The spectra from our models show a similar decay. The transition between the two regimes can also be detected.

4 A case study

4.1 General aspects of the sea breeze circulation

A case study of 29 July 1995 was selected because on that day no other large scale weather systems passed the model domain. Due to the temperature differences between land and sea a sea breeze circulation developed. A typical length scale of this mesoscale weather phenomenon is 100 km, so the circulation is expected to stay within the model domain. The time scale is 24 hours, but due to the limited forecast period of 12 hours only the daytime part of the circulation is studied. The forcing is rather slow and thus suitable for the first experiments with the high resolution model.

After sunrise the differential heating between land and sea causes a low level air flow from sea to land with a return flow aloft. It is obvious that the circulation is driven by diabatic heat sources, but also the Coriolis force is an important parameter. The Coriolis force accounts for the change in the flow direction during the day. After a sea breeze cycle the u- and v-components of the wind have approximately the same direction as in the beginning.

A remarkable feature is the sea breeze front which can be recognized as a convergence zone on wind charts. Other characteristics of the sea breeze front are the temperature jump of a few degrees and the increase in the specific humidity. Along the sea breeze front convective clouds can be observed. The sea breeze front is formed when the synoptic winds are weak and when there is sufficient short wave radiation. In the selected case both ingredients are available. Seaward synoptic winds keep the front in the coastal area and intensify the circulation. Conversely landward synoptic winds force the front more inland.

Finally, it should be noted that the observation network determines the minimum scales of the sea breeze circulation which can be seen. In the Netherlands the resolution of the observations at the surface is about 30 kilometer, so it is impossible to verify the smallest scales of the model.

4.2 Sensitivity for diffusion

In order to get some insight in the desired magnitude of the horizontal diffusion coefficients in relation to the spectral behaviour, a few experiments are conducted. The VHR model is run in the configuration in which the

best results can be expected i.e. Eulerian advection and doubly nested. The strategy of nesting and the choice for the Eulerian or semi-Lagrangian advection scheme will be discussed in section 4.3 and 4.4. At first the model is run

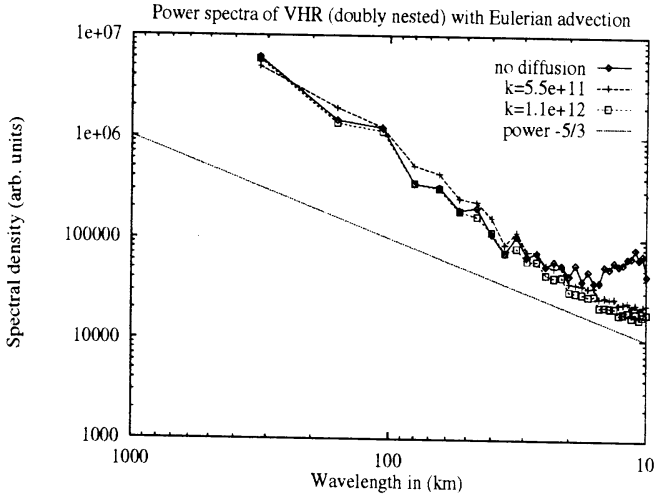

Figure 2: Spectra of the zonal wind component at model level 16 with varying horizontal diffusion coefficients. Data are based on a 12 hours forecast valid at 1800 UTC

without horizontal diffusion. In Fig. 2 the spectrum of the zonal component of the wind at the lowest model level is presented. The data are based on a case-study of 29 July 1995 as previously described in 4.1. The wind fields represent a 12 hours forecast and are valid at 1800 UTC. On the horizontal and the vertical axis the wavelength in meters and the spectral density in arbitary units are defined, respectively. Because the interesting feature is the distribution of the spectral energy over the wavelengths, it should be noted that the spectra do not represent energies in terms of Joules. With no diffusion the spectral line has an unrealistic decay. At smaller scales the energy-cascade is blocked, because effective dissipation is lacking.

The model is run subsequently with an implicit fourth order diffusion scheme. For the horizontal diffusion coefficient k=5.5e+11 and k=1.1e+12 are chosen. The spectral lines are now in accordance with the theory of the inertial subrange Tennekes (1972) [9] and reveal a $-5/3$ power law. The diffusion scheme effectively damps the smaller scales with a size of about

2-4 grid cells. Due to the numerical dissipation energy is extracted from the system at the small scales. Because of the interaction in the energy cascade the larger scales are also influenced. As a result the whole spectrum is more realistic.

Another interesting topic is whether the meteorological development influences the spectral distribution of energy. Therefore data of the same run is analyzed from another point of view. The meteorological situation as explained in 4.1, is a local weather phenomenon with a characteristic length scale of about 100 km. A secondary circulation driven by a temperature forcing between land and sea provides energy to the flow. The sea breeze

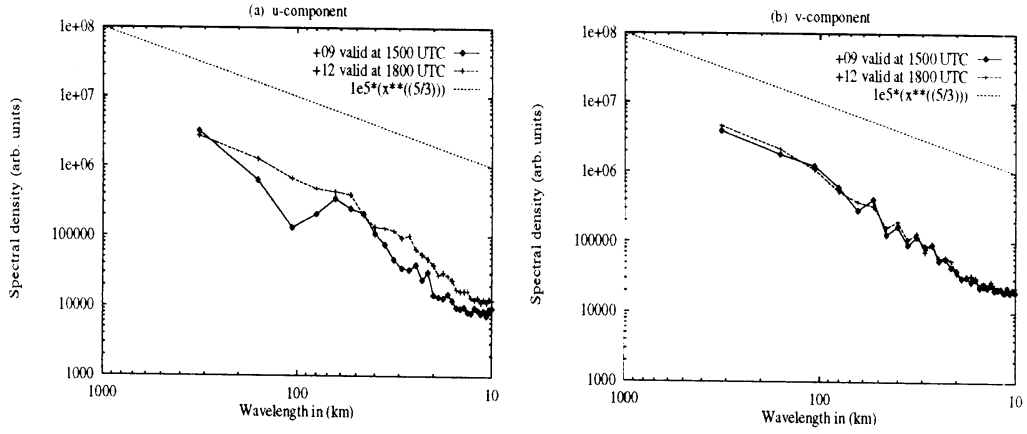

Figure 3: Effect of sea breeze on spectra of 29 July 1995. (a) u-component (b) v-component

circulation leads to a flow in a plane perpendicular to the coast, in our case this means that u-component of the wind is mainly affected. In Fig. 3a the spectrum of the zonal component of the wind at the lowest model level is presented. Around scales of 100 km energy is fed into the system. Three hours later when the forcing has become less dominant, the energy input at scales of 100 km has ceased. The energy is redistributed and transported to smaller scales, which is typical for 3-D turbulence in the boundary layer. As shown in Fig. 3b it is obvious that the spectra of the meridional components of the wind are less influenced by the sea breeze circulation. At 1500 and 1800 UTC the spectrum is flat and almost according to the $-5/3$ power

law. The v-component of the flow is hardly modified, because the forcing is parallel the Dutch coastal zone and headed in North-South direction.

4.3 Eulerian versus semi-Lagrangian advection scheme

Further experiments are conducted with a semi-Lagrangian and an Eulerian advection scheme. At first the choice for the horizontal diffusion coefficient is based on the scaling down principle (see formula 9). For VHR this gives a horizontal diffusion coefficients of k=1.66e+11 and k=3.52e+11 for the Eulerian and semi-Lagrangian scheme, respectively. It is obvious that for a clean comparison between the two advection schemes, the model runs should be made with equal horizontal diffusion coefficients. It should be noted that in both cases the implicit fourth order scheme was used. The time step for the dynamical scheme is 30 and 120 seconds for the Eulerian and semi-Lagrangian advection, respectively. The physics is performed after three timesteps in the Eulerian scheme, so the time step of the physical processes is effectively 120 seconds, which is the same value as for the semi-Lagrangian scheme.

The fourth order implicit diffusion scheme has a e-folding time of 0.05 hours, so it takes 3 minutes before the shortest waves of two grid cells are damped with a factor 1/e. From the section 4.2 we know that the spectra near the surface are strongly influenced by the sea breeze effect. In order to exclude the consequences of this phenomenon, spectra on mid-tropospheric level are studied. In Fig. 4 the computed spectra of model level 16 (400 hPa) for the case-study of 29 July 1995 can be found. V20 gives reasonable results for both semi-Lagrangian and Eulerian advection. Note that the spectral lines have a -3 and -5/3 power law decay for the large and small scales respectively. The semi-Lagrangian scheme gives suspicious results when the nesting of VHR in V20 is applied. The spectral lines reveal a lot of noise. Up to scales of 20 km there is an energy block which sharply drops at the tail of the spectrum. The energy in the middle of the spectrum corresponds with waves and spikes occuring in two bands. The Eulerian scheme has a much smoother picture without any noise.

Since spectral analysis on mid-tropospheric level does not tell the whole truth, and we procede with a study of the behaviour of the 10 m wind. The results are verified subjectively with observations. The doubly nested Eulerian run in Fig. 5 shows the 9 hours forecast of the 10 m wind and

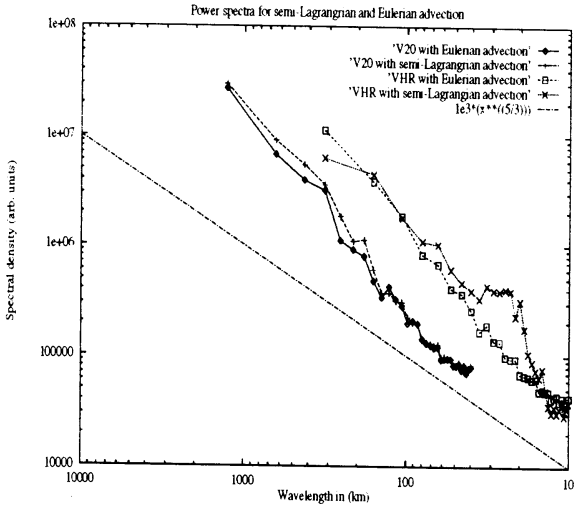

Figure 4: Spectra of predicted u-component fields. V20 and VHR +9 and +15 hours forecast, respectively, both valid at 1500 UTC on 29 July 1995

the surface observations at 1500 UTC. The observations of the wind are marked by circles. The inner blackening of the circle corresponds with the total amount of observed clouds. In the coastal zone between 4E, 52N and 5E, 53 N a typical seabreeze circulation is recognized. The surface wind is headed towards the coast and inland a convergence zone is found. Also the wind channelling over the IJsselmeer (the large former sea arm extending to the centre of the country), as reflected in both speed and direction, is subjectively verified by observations. Over the inland area, however the direction is too much backed. This can be explained from the physics of the model in combination of the low vertical resolution.

In Fig. 6 the similar result with the semi-Lagrangian scheme is presented. The sea breeze phenomenon is depicted as well as spurious waves. It is obvious that the model output contains non realistic noise. In order to improve the result with the semi-Lagrangian scheme further experiments are carried out. The horizontal diffusion coefficients are increased with a factor 10 and specified as a function of height. Maximum horizontal diffusion is chosen in the upper troposphere

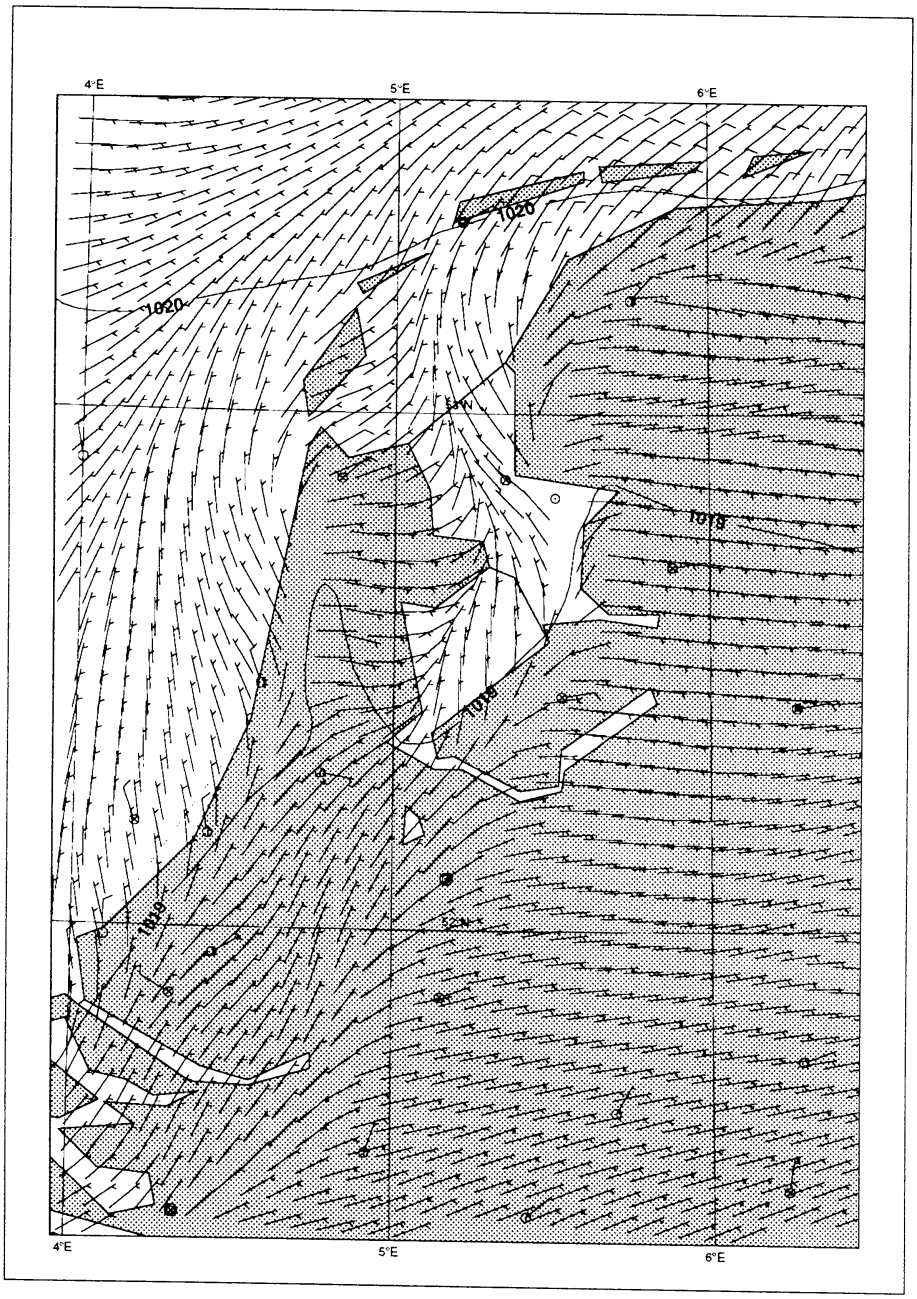

Figure 5: 10 m wind, doubly nested VHR 9 hours forecast, valid at 1500 UTC with Eulerian advection.

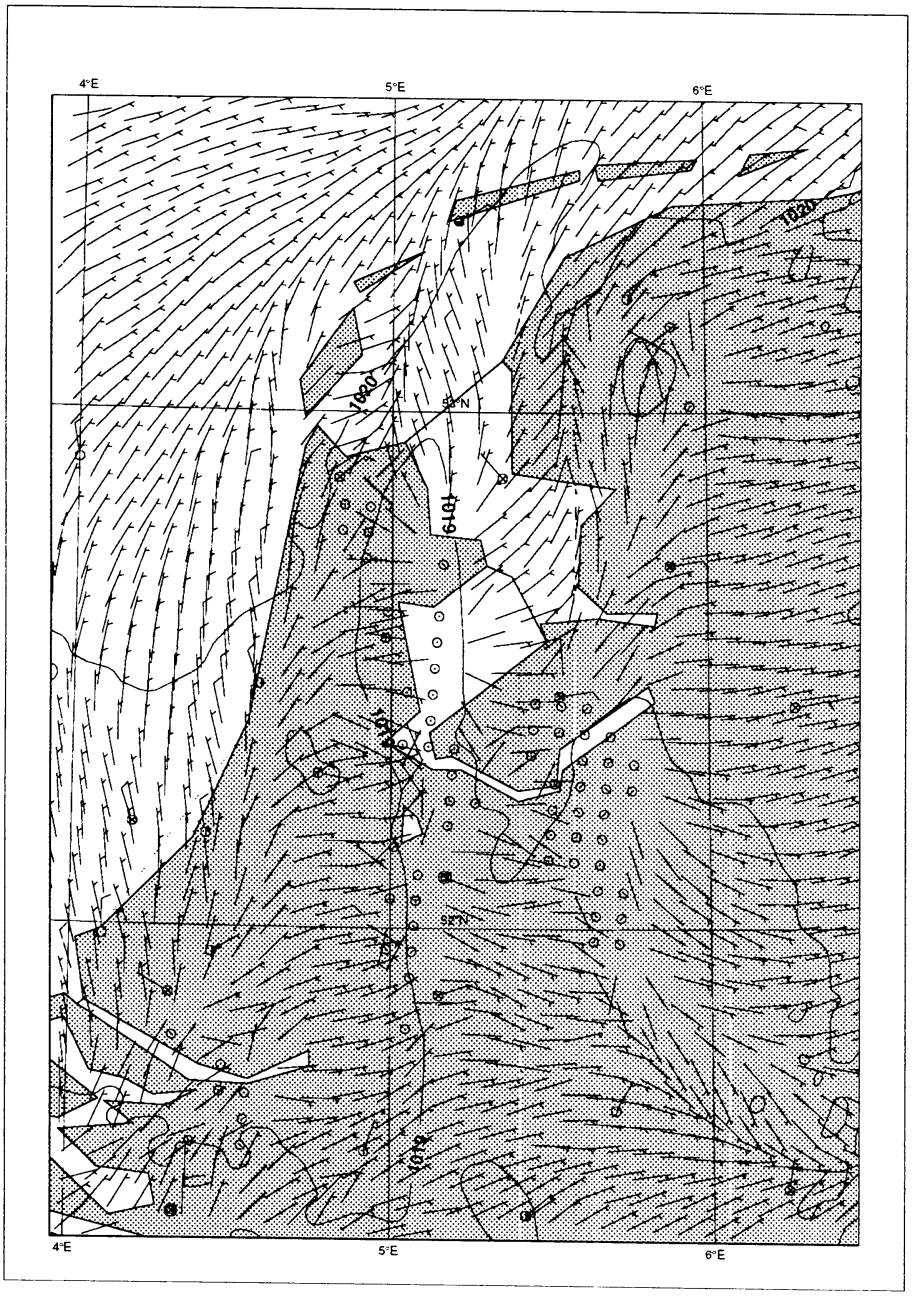

Figure 6: 10 m wind, doubly nested VHR 9 hours forecast valid at 1500 UTC with semi-Lagrangian advection

to damp the unwanted small scales. With the modified setting the 10 m wind chart, presented in Fig. 7 improves significantly and becomes comparible with the results of the Eulerian scheme. As shown in Fig. 7 the surface pressure field has become much smoother over the area of the Netherlands. When the spectrum of model level 16 is studied again, the energy block has not disappeared. In the corresponding wind field in Fig. 8 waves with a wavelength of 50-80 km are present, but also smaller spurious waves are recognized. The observations which do not match exactly in time, deviate from the model values at the specific locations. Together with the energy block in the spectral decay this is an indication that the predicted windfields reveal unrealistic phenomena. In order to get rid of these spurious waves the time step is decreased to 30 seconds for all processes. Unfortunately the noise does not disappear. The spectrum of the Eulerian run reveals a realistic decay, but the wind chart of model level 16 also shows a wind jump. It is not clear if this phenomenon is realistic and therefore the output of the larger scale model and the nesting strategy are studied in more detail.

4.4 Impact of the stepsize of nesting

In Fig. 9 the 15 hours forecast of the wind at model level 16 of the V20 model is presented. The run is made with the two available advection schemes and similar results are produced. The spectral decay is according to the theory. The wind at this model level of about 400 hPa varies significantly above the Netherlands and the wind pattern reveals a saddle point. Further a zone with a sharp windshift is recognized in the chart. This is confirmed by the observations which are marked with small circles. The sharp windshift is a frontal zone which is connected to a developing thunderstorm in the Northern part of the Netherlands. In the area where the Northern boundary of VHR is situated the wind changes over a range of 40 km from Southwest to Northwest to South. The V20 chart looks like it may have some 2-grid (or 4-grid) waves on it just where the Northern boundary is going to be for VHR. In that area the wind is coming from all directions and the saddle point might introduce noise into smaller scale model when the lateral boundaries are prescribed.

An important issue is whether the intermediate V20 model is strictly necessary to produce mesoscale forecasts, because running an extra model requires more computer resources. Therefore VHR is directly embedded in V55 and the model is rerun with the Eulerian and the semi-Lagrangian ad-

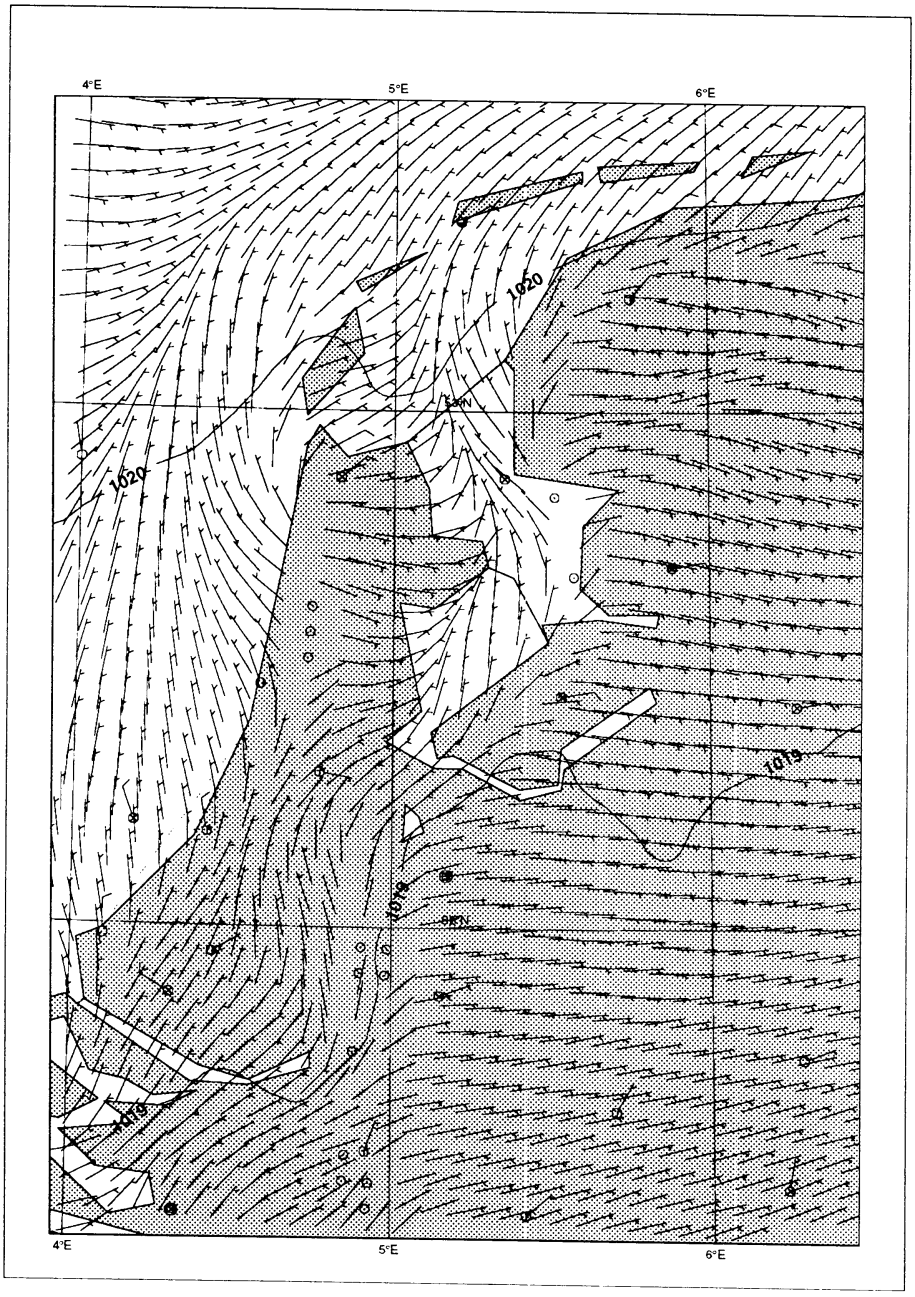

Figure 7: 10 m wind, doubly nested VHR 9 hours forecast valid at 1500 UTC with semi-Lagrangrian advection with increased horizontal diffusion

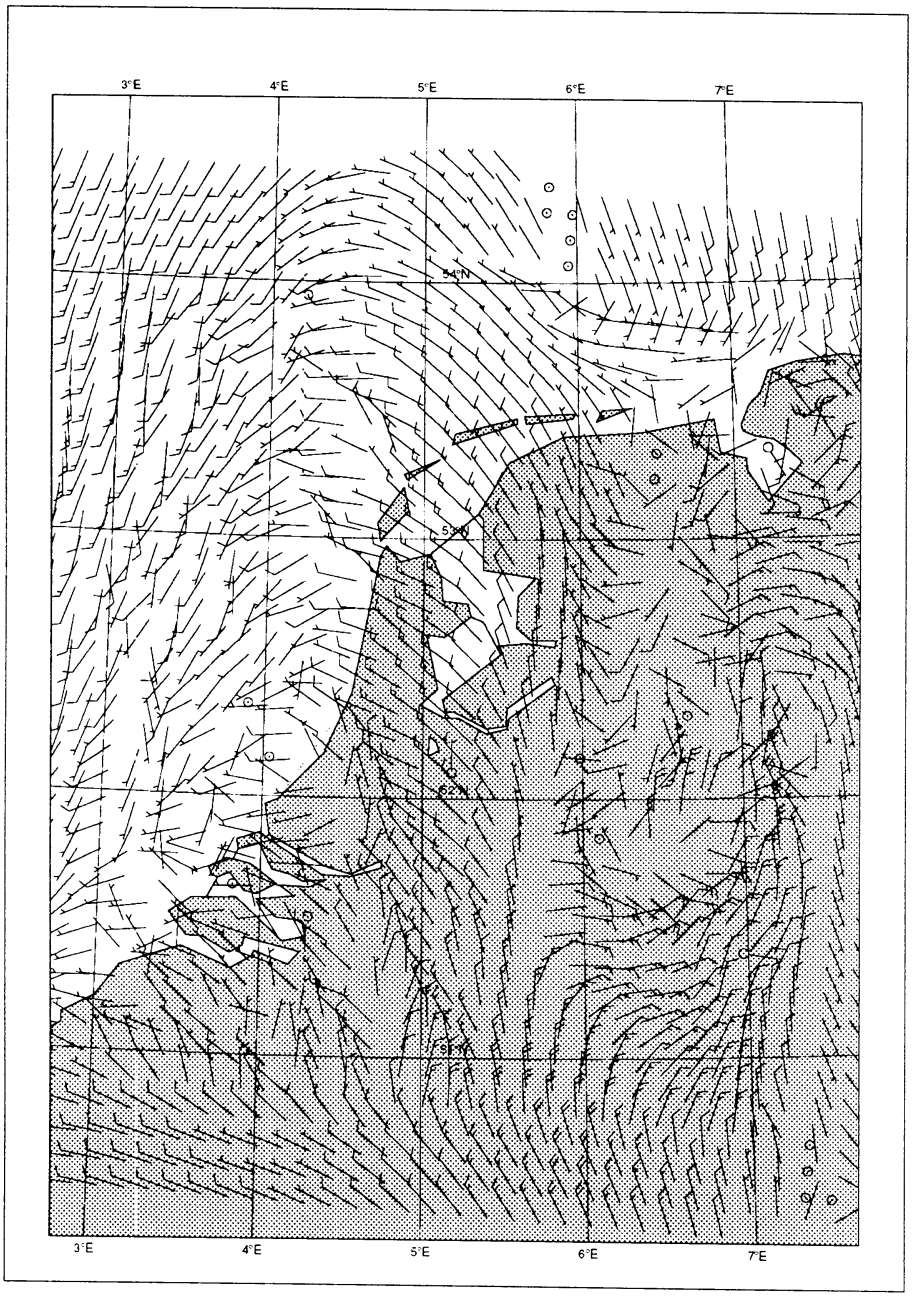

Figure 8: Wind at model level 16 (400 hPa), doubly nested VHR 9 hours forecast valid at 1500 UTC with semi-Lagrangrian advection with increased horizontal diffusion and upper air observations from radiosondes at 1800 UTC

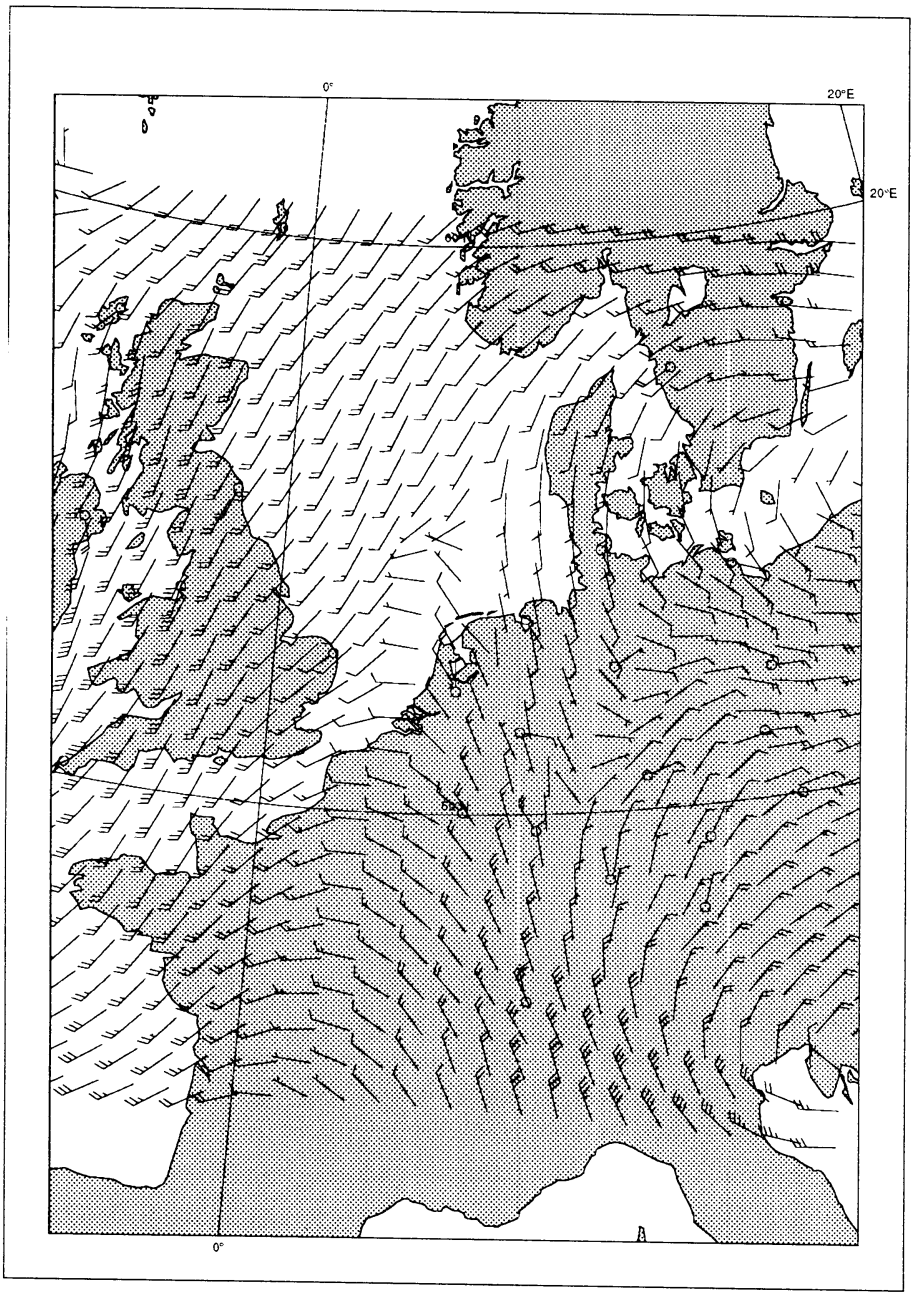

Figure 9: Winds at model level 16 (about 400hPa), calculated from the V20 model for 15 hours run valid at 1500 UTC and upper air observations from radio sondes at 1800 UTC

vection schemes. The diffusion coefficients and time steps are derived by downscaling using relation (9). First it should be noted that in the coarse model no mesoscale circulation is recognized. The nested runs provide additional information of the phenomenon at the smaller scales. The Eulerian scheme gives almost the same results with the doubly nested run. The semi-Lagrangian scheme depicts the sea breeze effect but also spurious waves are found in the windfield. The spectral analysis reveals noise at scales of 40-60 km. Again the results become more realistic when horizontal diffusion is increased. It is clear that the semi-Lagrangian scheme is more sensitive to noise than the Eulerian scheme.

In the fields of the V55 model waves are detected with a typical wavelength of 2-4 grid cells. These small scale waves belong to the tail of the spectrum of the V55 model. However when this data is used to prescribe the lateral boundaries for the nested model with a resolution of 0.05 degrees, it causes noise. In order to create proper boundary conditions the waves of 2-4 grid cells should be removed from the 0.55 degrees data. In that case only the large scale slowly varying data is used for the interpolation to the nested model. The removal of the 2-4 grid point waves was accomplished by filtering the operational fields. Instead of allowing more horizontal diffusion, this is an attractive method to remove the detailed information from the large scale model. The model output, which is used operationally, remains unaffected and the nested model receives noise free boundary information without 2-4 gridpoint parasitic waves from the coarse mesh data.

In Fig. 10 the results are presented of the directly nested very high resolution model. The lateral boundaries are derived from filtered V55 fields. In the data waves with a wavelength shorter than 2 degrees longitude-latitude are removed. A semi-Lagrangian scheme was used to solve the dynamic part of the model. The horizontal diffusion is specified per level. At the lowest level k=35.1e+11 is taken, the following levels have more diffusion. In fact the coefficients are chosen as in the experiment of the doubly nested semi-Lagrangian run. The e-folding time was 0.16 hours. From Fig. 10 it becomes obvious that the result is similar to that run. In Fig. 11 the wind field at model level 16 (about 400 hPa) is presented. The spurious waves have dissapeared, but two zones with wind jumps are recognized. These zones can also be detected in the larger scale model (see Fig. 9). They are realistic and probably connected with the developing thunderstorm.

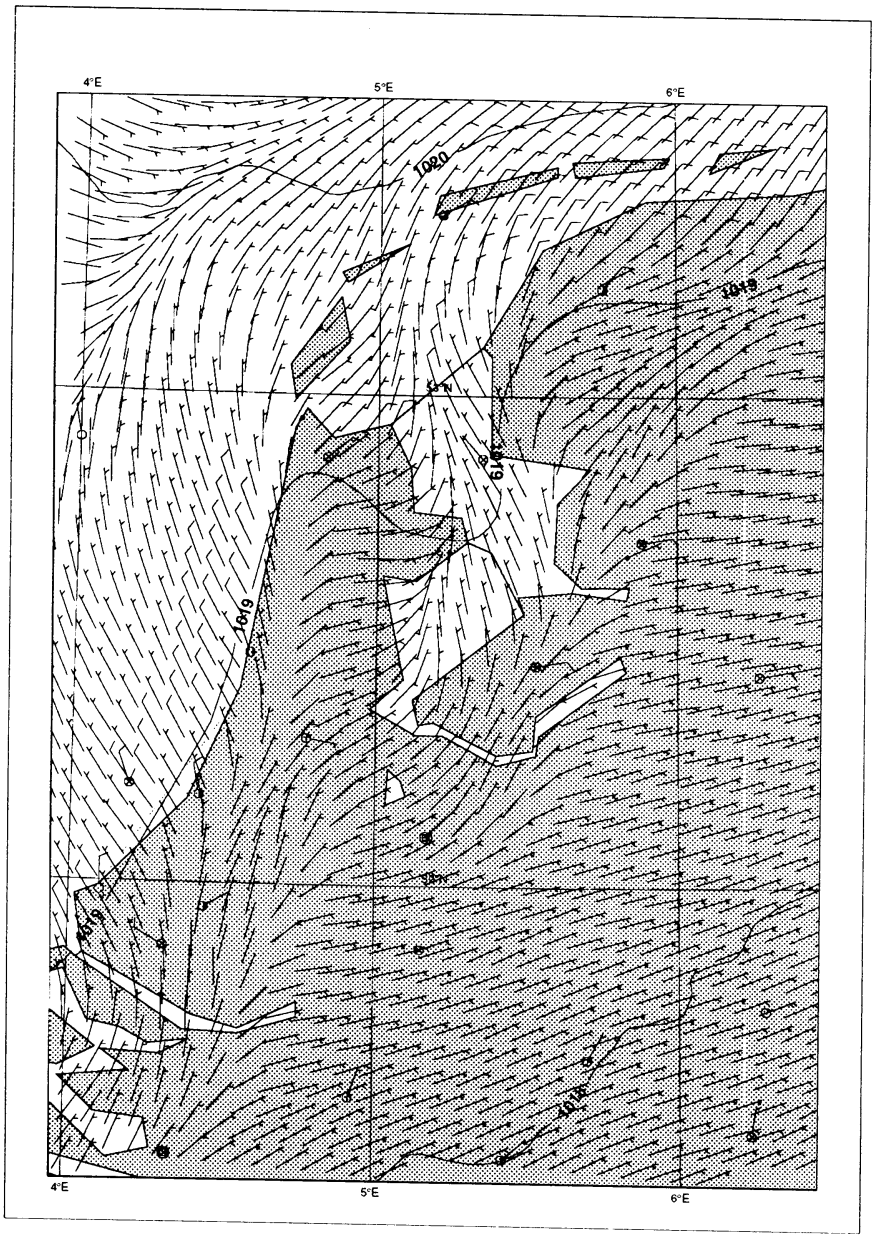

Figure 10: Directly nested run with filtered boundary conditions for 9 hours run valid at 1500 UTC with semi-Lagrangian advection

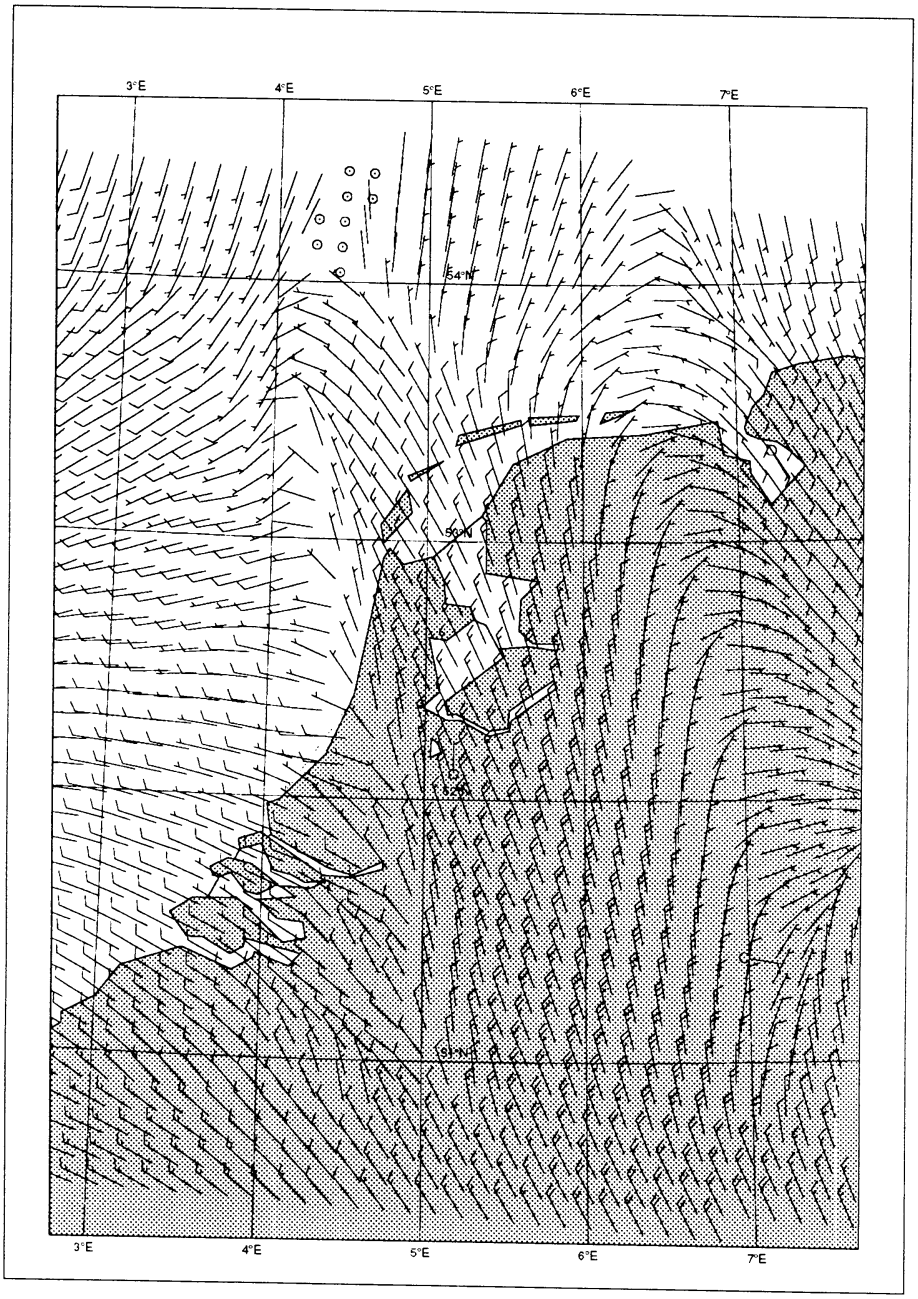

Figure 11: Wind at model level 16 (400 hPa) from the directly nested run with filtered boundary conditions for 9 hours run valid at 1500 UTC with semi-Lagrangian advection

4.5 Meteorological details with the most suitable model

The directly nested model with the filtered boundaries and the semi-Lagrangian advection scheme give satisfying results and therefore the model output is studied in more detail.

In Fig. 12 the time serie of the wind force, wind speed and 2m temperature is given for Valkenburg. Valkenburg is a military airport, close to The Hague and is situated near the North sea coast. When a secondary circulation, driven by the temperature contrast between land and sea occurs, it will certainly affect Valkenburg. A disadvantage of this choice is the lacking of upper air observations at that time. Therefore the model output at the surface are studied. The observations are ten minutes averages of the wind at 10 m and the temperature at screen height. In the model Valkenburg is treated as a land point and modeloutput is available every 120 sec which is equal to the timestep.

In the observations the wind is weak and variable in the first hours. The onset of the seabreeze effect is at 1100 UTC. The wind veers from easterly direction of 50 degrees to northerly direction of 350 degrees. At the same time there is an increase in the wind speed and a jump in the temperature curve. The model reveals the same phenomena, but there is a phase error of one and a half hour. Further the wind speed is underestimated after the passage of the sea breeze front. It is not clear whether the roughness length in the model is representative for the area where the wind comes from. The temperature is underestimated by the model during the first hours. This might be the reason why the seabreeze circulation started too late. An explanation for the slow heating is that the first soil layer is too thick, resulting in a slow response to the increasing short wave radiation.

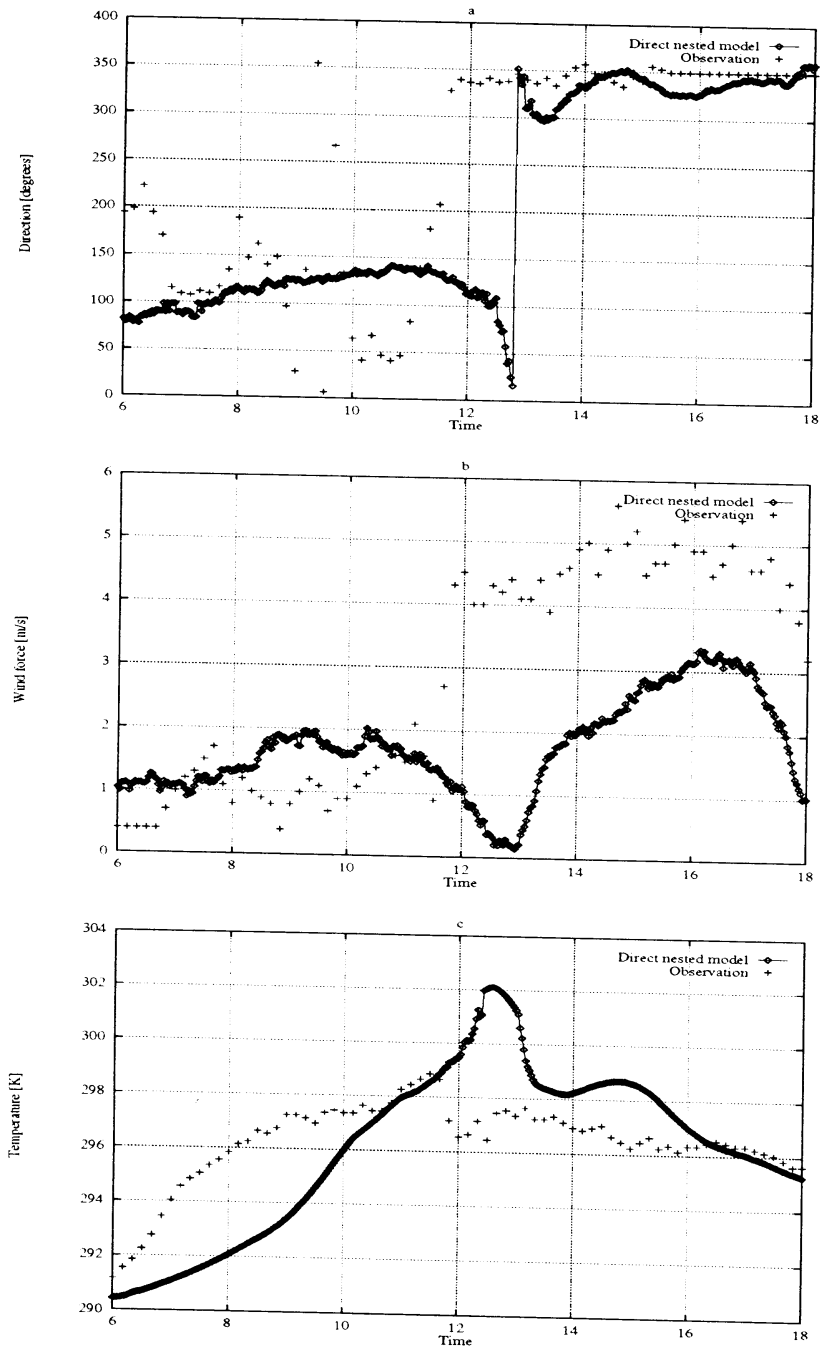

Figure 12: Timeseries of (a) Wind direction [degrees], (b) Wind speed [m/s] and(c) 2m temperature [C] at Valkenburg 29 July 1995

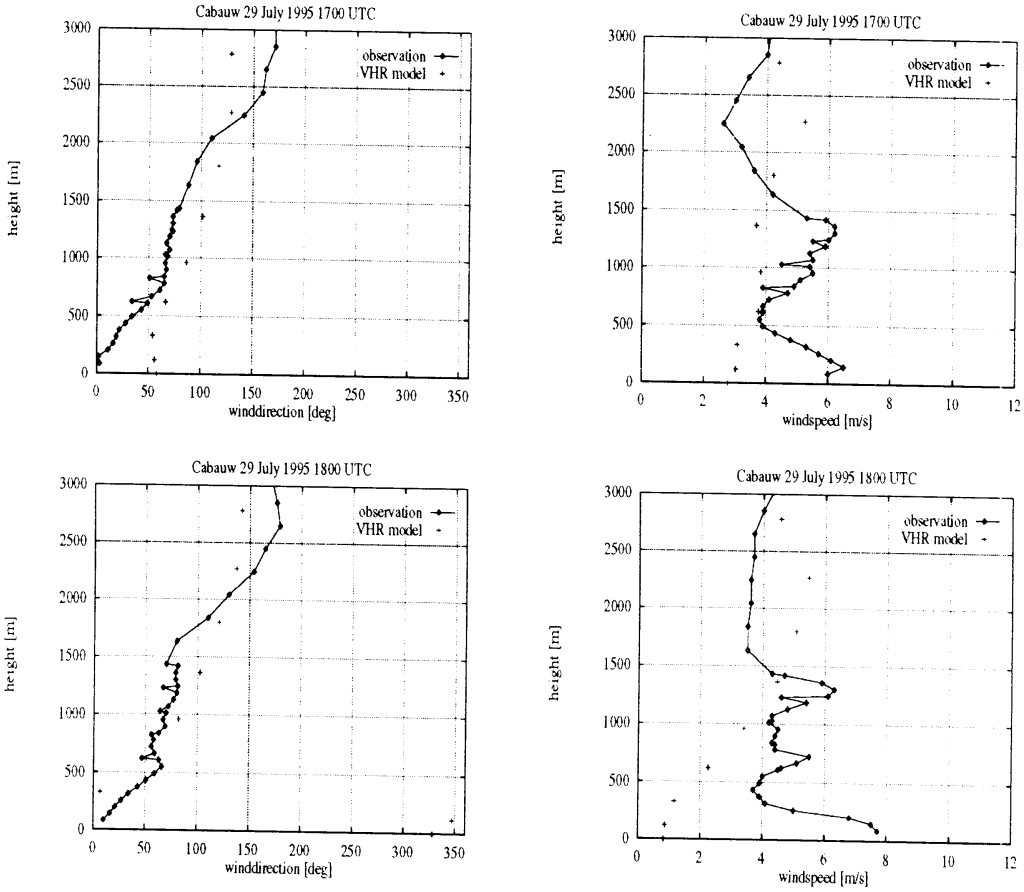

Figure 13: profiles of wind direction [degrees] (left) and speed [m/s] (right) at Cabauw valid at 1700 (up) and 1800 (down) UTC on 29 July 1995

The seabreeze front moves further inland and passes Cabauw (40 km from the coast) between 1700 and 1800 UTC. In Cabauw upper air observations are available from a windprofiler. In Fig. 13 the vertical profiles of wind direction and speed at 1700 and 1800 UTC are presented. Note that the model levels of VHR can be easily recognized. The lowest model level is at about 100m, the next at 300 m and so on. In appendix A a full list of the model level heights for Cabauw at that time is given. From first sight it is obvious that the windspeed is underestimated by the model at the lowest levels, but is overestimated above 1500 m. The predicted wind direction has

a better score. In the observations of 1800 UTC the windspeed has increased near the surface and also the wind direction changes abruptly at 500 m. This is explained by the seabreeze effect, because the wind comes from northerly directions and increases in the layer from the surface to 500 m height. The model has difficulties to represent details of the seabreeze effect properly. However from the timeseries it is known that VHR has phase error and the occurence of the seabreeze is presumably beyond the forecastperiod of 12 hours. Further the model has a low resolution in the vertical, which impacts on the simulation the atmospheric boundary layer processes.

5 Conclusions and recommendations

In this report the meteorological fields from a high resolution NWP have been studied. The model is able to generate mesoscale weather phenomena such as land-sea breezes. In our research we restrict ourselves to one case-study where the circulation remained in the domain and where the external forcing was determined by a temperature difference between land and sea. Spectral analysis is applied to meteorological fields from a high resolution NWP. At scales not exeeding more than 50 km the zonal velocity spectrum approaches $k^{-5/3}$ behaviour, while at the smaller scales the spectral slope levels off.

Increasing the horizontal diffusion affects the spectral behaviour of the meteorological fields. Detected numerical noise can be suppressed by increasing the horizontal diffusion coefficient. Consequently the spectral decay becomes more realistic, but the mesoscale phenomenon can be still recognized. In the chosen case-study the forcing which modifies the flow is stable and vanishes slowly during the day. In other situations where instantaneous forcings play an important role, the horizontal diffusion should not smooth the contributions of the physical processes.

Scaled down coefficients for horizontal diffusion did not give the proper results. Especially the semi-Lagrangrian scheme is very sensitive and revealed noise in the fields. Therefore the diffusion is increased and the results do improve. In order to make a clean comparison between the two schemes, experiments are conducted with the same fourth order diffusion scheme with equal horizontal diffusion coefficients. Both advection schemes give reasonable simulations of the sea breeze effect and of the wind jump in the upper air.

The nested models are sensitive for parasitic waves of the course mesh model which provides the boundaries. When the parasitic waves are removed artificially by application of a high frequency filter, the embedded model will benefit from this approach. Even the semi-Lagrangian scheme, which is more sensitive for discrepancies in the inner model improves when the boundary fields are filtered.

It is recommended to proceed with further research on the VHR model embedded in the V55 model with the semi-Lagrangian scheme and the filtered boundary information. More runs in different meteorological situations are necessary. Attention should be paid to the performance of the physical parametrizations. Further, more research is required about the in- and out-

flow of data from the high resolution model. Perhaps the two-way nesting method is an attractive alternative for the used one-way nesting method.

6 Acknowledgements

Drs. G. Cats and Drs. A.F. Moene are thanked for giving practical support in running the models at KNMI and for the generation of stimulating ideas. Dr. J.R.A. Onvlee is thanked for her critical reading of the manuscript. Dr. H.J.J. Jonker and Dr. M.H.P. Ambaum are acknowlegded for giving advise on the mathematical aspects. Dr. A. McDonald from the Irish Meteorological Office is gratefully thanked for his advisory comments about the experiments with the Eulerian and semi-Lagrangian advection schemes. Ir. H. Klein Baltink is kindly thanked for providing the windprofiler data of Cabauw.

Prof. Dr. B. Holtslag, who is my supervisor is thanked for his constructive ideas. Dr. ir. B. Wichers Scheur, who is my deputy-supervisor is acknowlegded for his contribution to this research. Dr. A.J. van Delden and Drs. A.B.C. Tijm, both from Utrecht University are thanked for their criticism on the draft of this report.

References

[1] Clark, Terry L., William D. Hall (1991) Multi-domain simulations of the time dependent Navier-Stokes equations: Benchmark error analysis of some nesting procedures. *J. Comput. Phys.* 92, 456-481.

[2] Eerola, K. (1993) Experimentation with second and fourth order horizontal diffusion schemes *HIRLAM Technical Report* 13, 27p.

[3] Gustafsson, N, (1991) The HIRLAM model. *Seminar Proceedings on Numerical Methods in Atmospheric Models.* Volume II, 115-146 [Available from ECMWF, Shinfield Park, Reading England]

[4] Haugen, J. E., (1991) Implicit normal mode initialization and implicit Daley time integration in the HIRLAM model *Internal report* 20 p [Available from Det Norske Meteorologike Institutt, Postboks 43 Blindern, 0313 Oslo 3, Norway]

[5] McDonald, A., and J. Haugen (1992) A two-time-level, three-dimensional semi-Lagrangian, semi-implicit limited-area gridpoint model of the primitive equations *Mon. Wea. Rev.* 120, 2603-2621

[6] McDonald, A., and J. Haugen (1993) A two time-level, three-dimensional, semi-Lagrangian, semi-implicit limited-area gridpoint model of the primitive equations. Part II: Extension to hybrid vertical coordinates. *Mon. Wea. Rev.* 121, 2077-2087.

[7] Nastrom, G.D., K.S. Gage and W.H. Jasperson (1984) Kinetic energy spectrum of large- and mesoscale atmospheric processes. *Nature* 2, 36-38.

[8] Nielsen, Niels W., Bent H. Sass and Jess Jorgensen (1995) Mesoscale forecasts with an atmospheric Limited Area Model. *Meteorol. Appl.*, 2, 353-361.

[9] Tennekes, H., and J.L. Lumley (1972) A first Course in Turbulence. *MIT Press, Cambridge, Mass* 300 p.

[10] Wieringa, J. (1992) Updating the Davenport roughness classification. *J.Wind Engin.Industr.Aerodyn.* 41, 357-368.

A a and b coefficients hybrid coordinate system

model level	height [m]	a(i)	b(i)
11	11921	16365.8085937500	0.0736913109
12	11041	16381.3125000000	0.1049492359
13	10201	16044.6093750000	0.1417225647
14	9395	15388.4335937500	0.1835724068
15	8615	14455.3945312500	0.2299459076
16	7859	13295.4062500000	0.2802119827
17	7138	11963.2578125000	0.3336901855
18	6434	10516.3164062500	0.3896736526
19	5749	9012.3085937500	0.4474452209
20	5094	7507.2773437500	0.5062873840
21	4483	6053.6289062500	0.5654854202
22	3885	4698.3164062500	0.6243244553
23	3322	3481.1435546875	0.6820794678
24	2781	2433.1872558594	0.7379998016
25	2268	1575.3476562500	0.7912860870
26	1801	917.0192871094	0.8410614014
27	1364	454.8876953125	0.8863358307
28	963	171.8450622559	0.9259645081
29	620	36.0317840576	0.9585992432
30	332	0.0000000000	0.9826333618
31	121	0.0000000000	0.9961407471

Coefficients of the hybrid coordinate system of the models. In the second column the model heights in meters are given for Cabauw (51.97 N 4.93 E) The surface pressure P_s is 1018.5 hPa